数理解析研究所講究録
第1608巻 2008年 180-188

回転系における平面ポアズイユ流の安定性と解の分岐

京都大学・工学研究科　永田雅人 (Masato Nagata),
増田周一 (Shūichi Masuda)
Graduate School of Engineering,
Kyoto University

概要

We analyse the stability of plane Poiseuille flow with a streamwise system rotation. It is found that the instability due to two-dimensional perturbations, which sets in at the well known critical Reynolds number, $R_c = 5772.2$, for the non-rotating case, is delayed as the rotation is increased from zero, showing a stabilising effect of rotation. As the rotation is increased further, however, the laminar flow becomes most unstable to perturbations which are three-dimensional. The critical Reynolds number due to three-dimensional perturbations at this higher rotation case is of many orders of magnitude less than the corresponding value due to two-dimensional perturbations. We also perform a nonlinear analysis on a bifurcating three-dimensional secondary flow. The secondary flow exhibits a spiral vortex structure propagating in the streamwise direction. It is confirmed that an anti-symmetric mean flow in the spanwise direction is generated in the secondary flow.

1 Introduction

It is important to understand the stability of flows under a system rotation for both engineering and geophysical applications. Compared with a large number of investigations on plane Poiseuille flow with a spanwise system rotation (see Wall & Nagata (2006) and the references therein), the same flow with a streamwise system rotation has attracted less attention despite its importance in the geophysical context, such as instabilities of meridional flows across the equator. As far as the authors know even the linear stability of the laminar flow has not yet been analysed properly. It is only recently that experimental (Recktenwald *et al.* (2004)) and numerical (Oberlack *et al.* (2006)) investigations of turbulent plane Poiseuille flow with a streamwise rotation have been reported. The most striking feature among other turbulent properties reported is the generation of a mean flow in the spanwise direction.

Plane Poiseuille flow with a streamwise system rotation can be regarded as the narrow-gap limit of an annular Poiseuille flow between concentric rotating cylinders. As a special example of so-called spiral Poiseuille flow (Joseph(1976)), where the two concentric cylinders rotate independently (Chung & Astill (1977), Hasoon & Martin (1977), Takeuchi &Jankowski(1981) and Cotrell & Pearltein (2004, 2006)), the linear stability of the rigid-body rotation case with the radius ratio 0.5 has been studied by Meseguer & Marques (2002) with the result that the critical state is determined by the non-axisymmetric modes. Non-axisymmetric modes in annular Poiseuille flow correspond to three-dimensional modes in our plane geometry.

The purposes of the current paper are to identify the critical mode for the stability of plane Poiseuille flow with a streamwise rotation and to seek the origin of the spanwise mean flow.

2 Mathematical formulation

We consider a viscous incompressible fluid motion of a fluid with density ρ_* between two parallel plates with a gap width, $2d_*$, induced by a constant pressure gradient under the system rotation Ω_*. The orientation of the system rotation is parallel to the pressure gradient as shown in Fig.1. We take the

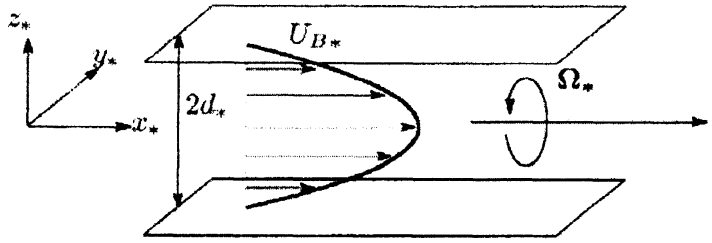

図 1: The configuration of the model

origin of the coordinate system on the midplane between the plates, with the x_*- and y_*-coordinates directing in the streamwise and spanwise directions, respectively and the z_*-coordinate being normal to the plates. Corresponding to the x_*-, y_*- and z_*-coordinates, we define the unit vectors $\boldsymbol{i}$, $\boldsymbol{j}$, and $\boldsymbol{k}$. The basic flow with a quadratic velocity profile, *i.e.* the plane Poiseuille flow, $U_{B*}(z_*)$, is not affected by the rotation. We are interested in investigating the stability of the basic flow and analysing the nature of a secondary flow which may bifurcate when the basic flow should lose its stability.

In order to non-dimensionalise the system we take d_* as the length scale, d_*^2/ν as the time scale, ν/d_* as the velocity scale and $\rho_*\nu^2/d_*^2$ as the pressure scale, where ν is the kinematic viscosity. Then, the equations of continuity and the conservation of momentum are written as

$$\nabla \cdot \boldsymbol{u} = 0 \tag{1}$$

and

$$\frac{\partial \boldsymbol{u}}{\partial t} + (\boldsymbol{u} \cdot \nabla)\boldsymbol{u} = -\nabla \Pi + \nabla^2 \boldsymbol{u} - \Omega \boldsymbol{i} \times \boldsymbol{u}, \tag{2}$$

where $\boldsymbol{u}$ is the velocity, Π is the pressure and Ω is the rotation number defined by

$$\Omega = \frac{2\Omega_* d_*^2}{\nu}. \tag{3}$$

The governing equations are to be solved subject to the no-slip boundary condition on the plates:

$$\boldsymbol{u} = \boldsymbol{0} \qquad \text{at} \qquad z = \pm 1. \tag{4}$$

Assuming that the basic flow $\boldsymbol{U}_B$ is unidirectional in the $x-$direction depending only on the $z-$coordinate when the imposed pressure gradient $\frac{\partial \Pi}{\partial x}$ is constant, we obtain

$$U_B(z) = \boldsymbol{U}_B \cdot \boldsymbol{i} = R(1 - z^2), \tag{5}$$

where we have used the value, $U_{0*} = U_{B*}(0)$, of the basic flow on the midplane $z = 0$ to define the Reynolds number

$$R = \frac{U_{0*} d_*}{\nu}. \tag{6}$$

The stability of the basic state as well as the development of a new flow field due to the loss of stability is governed by two non-dimensional parameters, R and Ω.

In order to analyse the stability of the basic state and to seek solutions other than the basic state we superimpose disturbances, $\hat{\boldsymbol{u}}$ and $\hat{\Pi}$, on the basic state.

$$\boldsymbol{u} = \boldsymbol{U}_B + \hat{\boldsymbol{u}}, \qquad \Pi = \Pi_B + \hat{\Pi}. \tag{7}$$

Substituting (7) into (1) and (2) we find that the disturbances satisfy the following equations.

$$\nabla \cdot \hat{\boldsymbol{u}} = 0, \tag{8}$$

$$\frac{\partial \hat{\boldsymbol{u}}}{\partial t} + (\hat{\boldsymbol{u}} \cdot \nabla)(U_B \boldsymbol{i} + \hat{\boldsymbol{u}}) + (U_B \boldsymbol{i} \cdot \nabla)\hat{\boldsymbol{u}} = -\nabla \hat{\Pi} + \nabla^2 \hat{\boldsymbol{u}} - \Omega \boldsymbol{i} \times \hat{\boldsymbol{u}}. \tag{9}$$

The no-slip boundary condition for $\hat{\boldsymbol{u}}$ is given by

$$\hat{\boldsymbol{u}} = \boldsymbol{0} \qquad \text{at} \qquad z = \pm 1. \tag{10}$$

For convenience the velocity disturbance $\hat{\boldsymbol{u}}$ is separated into the mean parts, $\check{U}(t,z)$ in the streamwise direction and $\check{V}(t,z)$ in the spanwise direction, and the residual $\check{\boldsymbol{u}} = (\check{u}, \check{v}, \check{w})^T$,

$$\hat{\boldsymbol{u}} = \check{U}(t,z)\boldsymbol{i} + \check{V}(t,z)\boldsymbol{j} + \check{\boldsymbol{u}}, \tag{11}$$

so that

$$\check{U}(t,z) = \overline{\hat{\boldsymbol{u}}} \cdot \boldsymbol{i} \quad \text{and} \quad \check{V}(t,z) = \overline{\hat{\boldsymbol{u}}} \cdot \boldsymbol{j}, \tag{12}$$

where the $xy-$average is indicated by an over-line. By definition the $xy-$average of the residual vanishes:

$$\overline{\check{\boldsymbol{u}}} = 0. \tag{13}$$

We anticipate that the mean parts, $\check{U}(t,z)$ and $\check{V}(t,z)$, are created by the Reynolds stress (see (19) and (20)).

The residual $\check{\boldsymbol{u}}$, which is solenoidal, is further separated into the poloidal and the toroidal parts as

$$\check{\boldsymbol{u}} = \nabla \times \nabla \times (\phi \boldsymbol{k}) + \nabla \times (\psi \boldsymbol{k}) = (\partial^2_{xz}\phi + \partial_y \psi, \partial^2_{yz}\phi - \partial_x \psi, -\Delta_2 \phi)^T, \tag{14}$$

where $\Delta_2 = \partial^2_{xx} + \partial^2_{yy}$. The total velocity field is now given by

$$\boldsymbol{u} = \boldsymbol{U}_B(z) + \check{U}(t,z)\boldsymbol{i} + \check{V}(t,z)\boldsymbol{j} + \nabla \times \nabla \times (\phi \boldsymbol{k}) + \nabla \times (\psi \boldsymbol{k}). \tag{15}$$

Note that (13) requires $\overline{\phi} = \overline{\psi} \equiv 0$.

The no-slip boundary condition (10) leads to

$$\check{U} = \check{V} = \phi = \frac{\partial \phi}{\partial z} = \psi = 0 \quad \text{at} \quad z = \pm 1. \tag{16}$$

After substituting (15) into (9) we operate $\boldsymbol{k} \cdot (\nabla \times \nabla \times$ and $\boldsymbol{k} \cdot (\nabla \times$ on (9) to obtain

$$\begin{aligned} \partial_t \nabla^2 \Delta_2 \phi + ((U_B + \check{U})\partial_x \nabla^2 + \check{V}\partial_y \nabla^2 - \nabla^4 - (U_B + \check{U})''\partial_x - \check{V}''\partial_y)\Delta_2 \phi \\ + \Omega \partial_x \Delta_2 \psi + \delta((\check{\boldsymbol{u}} \cdot \nabla)\check{\boldsymbol{u}}) = 0, \end{aligned} \tag{17}$$

$$\begin{aligned} \partial_t \Delta_2 \psi + ((U_B + \check{U})\partial_x + \check{V}\partial_y - \nabla^2)\Delta_2 \psi \\ -((U_B + \check{U})'\partial_y + \Omega \partial_x - \check{V}'\partial_x)\Delta_2 \phi - \epsilon((\check{\boldsymbol{u}} \cdot \nabla)\check{\boldsymbol{u}}) = 0, \end{aligned} \tag{18}$$

where the prime, $'$, denotes differentiation with respect to z.

The equations for the mean parts $\check{U}(t,z)$ and $\check{V}(t,z)$ can be obtained by taking the $xy-$ averages of the $x-$ and $y-$components, respectively, of (9):

$$\check{U}'' + \partial_z \overline{\Delta_2 \phi (\partial_{zx}^2 \phi + \partial_y \psi)} = \frac{\partial \check{U}}{\partial t}, \tag{19}$$

$$\check{V}'' + \partial_z \overline{\Delta_2 \phi (\partial_{zy}^2 \phi - \partial_x \psi)} = \frac{\partial \check{V}}{\partial t}. \tag{20}$$

3 Numerical methods

3.1 The linear analysis

Since the mean parts, $\check{U}(t,z)$ and $\check{V}(t,z)$, are created by the Reynolds stresses, where disturbances interact quadratically (see (19) and (20)), they do not participate in the linear analysis. Omitting $\check{U}(t,z)$, $\check{V}(t,z)$ and nonlinear terms $\delta((\check{\boldsymbol{u}} \cdot \nabla)\check{\boldsymbol{u}})$ and $\epsilon((\check{\boldsymbol{u}} \cdot \nabla)\check{\boldsymbol{u}})$ in (17) and (18), we obtain

$$\frac{\partial}{\partial t} \nabla^2 \Delta_2 \phi = \left(\nabla^4 + U_B'' \partial_x - U_B \partial_x \nabla^2\right) \Delta_2 \phi - \Omega \partial_x \Delta_2 \psi, \tag{21}$$

$$\frac{\partial}{\partial t} \Delta_2 \psi = (U_B' \partial_y + \Omega \partial_x) \Delta_2 \phi + (\nabla^2 - U_B \partial_x) \Delta_2 \psi. \tag{22}$$

In order to solve the equations above by the normal mode ansatz we expand ϕ and ψ using the Chebyshev polynomials $T_\ell(z)$ as follows:

$$\phi = \sum_{l=0}^{\infty} a_l (1-z^2)^2 T_\ell(z) \exp(i\alpha x + i\beta y + \sigma t), \tag{23}$$

$$\psi = \sum_{l=0}^{\infty} b_l (1-z^2) T_\ell(z) \exp(i\alpha x + i\beta y + \sigma t), \tag{24}$$

where σ is the growth rate and the factors, $(1-z^2)^2$ for ϕ and $(1-z^2)$ for ψ, are incorporated so that the boundary conditions

$$\phi = \frac{\partial \phi}{\partial z} = \psi = 0 \quad \text{at} \quad z = \pm 1 \tag{25}$$

are satisfied automatically. For numerical purposes the infinite series in (23) and (24) must be truncated by using only the first $(L+1)$ terms. The evaluation of (21) and (23) at the collocation points

$$z_i = \cos\left(\frac{i\pi}{L+2}\right), \qquad (i = 1, ..., L+1), \tag{26}$$

after (23) and (24) are substituted, leads us to the eigenvalue problem

$$A_{ij} x_j = \sigma B_{ij} x_j, \; x_j \in (a_l, b_l) \qquad (l = 0, 1, ..., L), \tag{27}$$

with σ as the eigenvalue. We solve (27) numerically by using the package DGVCCG of IMSL software library (Visual Numerics Inc. (1990)) which uses QZ algorithm. We find that $L = 20$ gives an accuracy which is far more than sufficient for our purpose.

3.2 The nonlinear analysis

Finite amplitude solutions are governed by (17), (18), (19) and (20) subject to the boundary conditions (16). Since the eigenvalue is a single complex number, *i.e.*, not a complex conjugate, we anticipate that the solution bifurcating from the linear critical state is of travelling-wave type. Therefore, we expand ϕ, ψ, $\check{U}$ and $\check{V}$ as

$$\phi = \sum_{l=0}^{L} \sum_{\substack{m=-M \\ (m,n)\neq(0,0)}}^{M} \sum_{n=-N}^{N} a_{lmn}\, f_l(z) \exp(im\alpha(x-ct) + in\beta y), \tag{28}$$

$$\psi = \sum_{l=0}^{L} \sum_{\substack{m=-M \\ (m,n)\neq(0,0)}}^{M} \sum_{n=-N}^{N} b_{lmn}\, g_l(z) \exp(im\alpha(x-ct) + in\beta y), \tag{29}$$

$$\check{U}(z) = \sum_{l=0}^{L} c_l\, g_l(z), \tag{30}$$

$$\check{V}(z) = \sum_{l=0}^{L} d_l\, g_l(z), \tag{31}$$

at the truncation level $(L, M. N)$. It can be shown that the mean parts, $\check{U}$ and $\check{V}$, do not depend on time for a travelling-wave solution The boundary conditions (16) are satisfied by taking

$$f_l(z) = (1-z^2)^2\, T_l(z), \tag{32}$$

$$g_l(z) = (1-z^2)\, T_l(z). \tag{33}$$

Evaluation of (17), (18), (19) and (20) at the same collocation points (26) that are used in the linear analysis after (28), (29), (30) and (31) are substituted into them leads us to the algebraic equation

$$A_{ij}x_j + B_{ijk}x_jx_k = 0,\ x_j \in (a_{lmn}, b_{lmn}, c_l, d_l, c). \tag{34}$$

The unknown vector components $a_{lmn}, b_{lmn}, c_l, d_l, c$ are determined by a Newton-Raphson iterative scheme. Although the number of unknowns is increased by one due to the inclusion of the unknown phase speed c, the number of unknowns and equations can be matched by fixing, for example, the imaginary part of one of the amplitude coefficients a_{lmn} at zero. This means physically that the flow is frozen at some instance (see Wall and Nagata (2006)). The deviation of the phase speed from the linear solution can be used as a nonlinear measure of the secondary flow.

The momentum transports in the streamwise and the spanwise directions,

$$\check{U}_\tau = \left.\frac{\partial \check{U}}{\partial z}\right|_{z=1} \tag{35}$$

and

$$\check{V}_\tau = \left.\frac{\partial \check{V}}{\partial z}\right|_{z=1}, \tag{36}$$

can also be used as nonlinear measures of the secondary flow. We select $(L, M, N) = (15, 5, 5)$ as a sufficiently accurate truncation level in the following calculations.

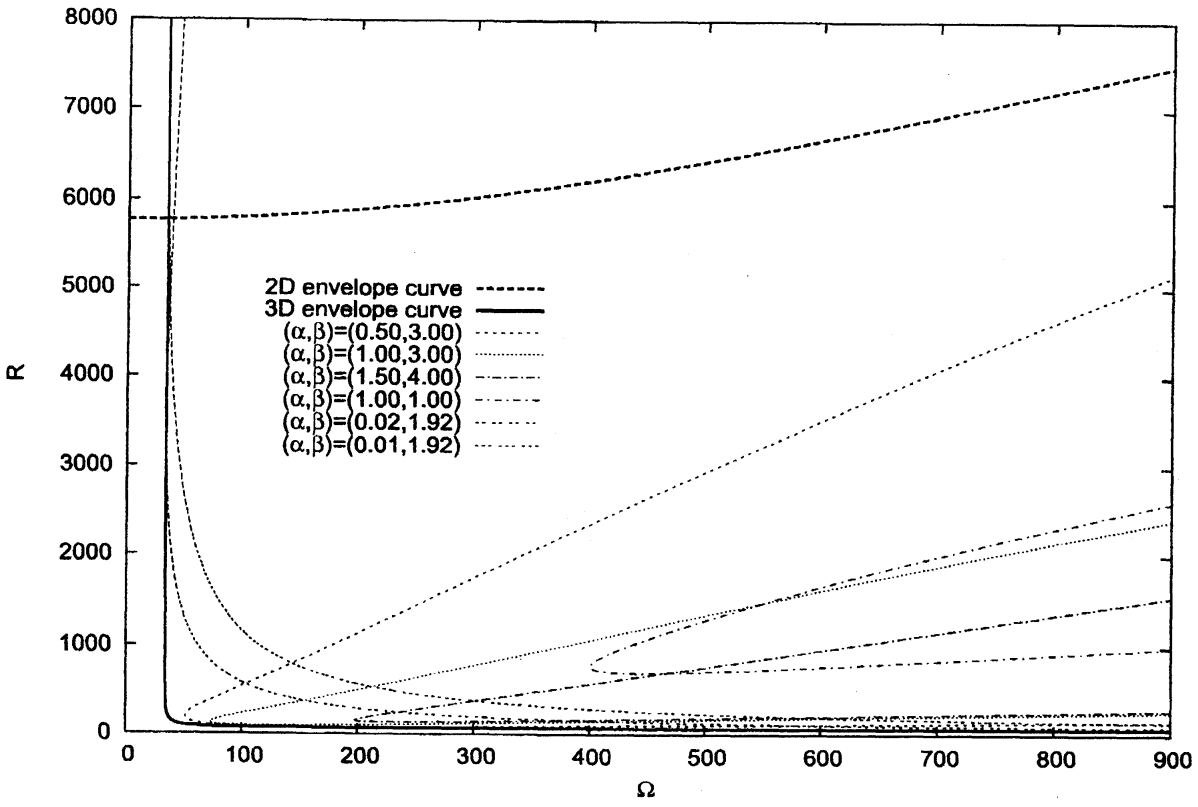

図 2: The neutral curves in the $\Omega - R$ plane for various wavenumber pairs. α varies along the 2D envelope curve with $\beta = 0$, while both α and β vary along the 3D envelope curve. The 2D envelope curve intersects the R−axis at $R = 5772.2$ with $\alpha = 1.02$. The 3D envelope curve seems to have asymptotes at large R and at large Ω.

4 Results

4.1 The linear analysis

Fig.2 shows the curves of $\Re[\sigma] = 0$ in the $\Omega - R$ plane for various wavenumber pairs (α, β). We can see from Fig.2 that the flow is unstable at a large Reynolds number against two-dimensional perturbations $(\beta = 0)$ for $\Omega \simeq 0$. We find actually that two-dimensional perturbations dominate for $\Omega \leq 33.923$ and that three-dimensional perturbations become responsible for instability for $\Omega 33.923$. Fig.2 indicates that the critical Reynolds number, R_c, decreases rapidly as Ω increases slightly over 33.923 and that it takes an almost constant value for large Ω. (In fact,$R_c = 66.50$ at $\Omega = 1000$, 66.46 at $\Omega = 2000$ and 66.45 at $\Omega = 3000$). When $\Omega > 500$ the streamwise wavenumber α of the three-dimensional perturbations corresponding to the critical Reynolds number decreases as Ω increases, while the spanwise wavenumber β remains at an almost constant value, $\beta \approx 2.5$. The existence of two asymptotic regimes for the three-dimensional perturbations, namely, $\Omega \simeq 33.923$ at large R and $R_c \simeq 66.45$ at large Ω, can be compared with those in the rigid-body rotation case of the spiral Poiseuille flow with the radius ratio 0.5 of the two cylinders (Meseguer & Marques (2002)) where the two regimes are determined by the non-axisymmetric modes with the azimuthal wavenumber $n = 5$ and $n = 6$.

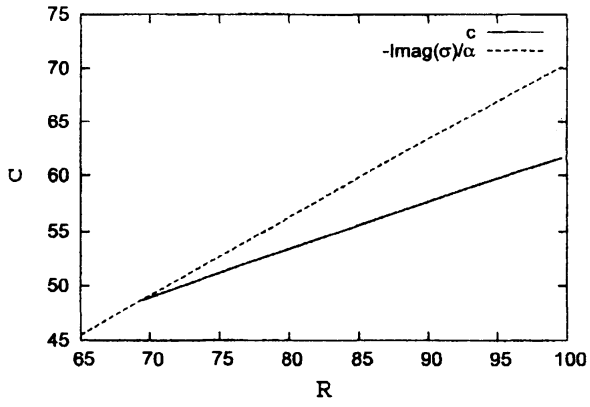

図 3: The phase speed with α=0.35, β=2.36, Ω=140. The solid curve indicates the nonlinear state whereas the dashed curve indicates the linear state.

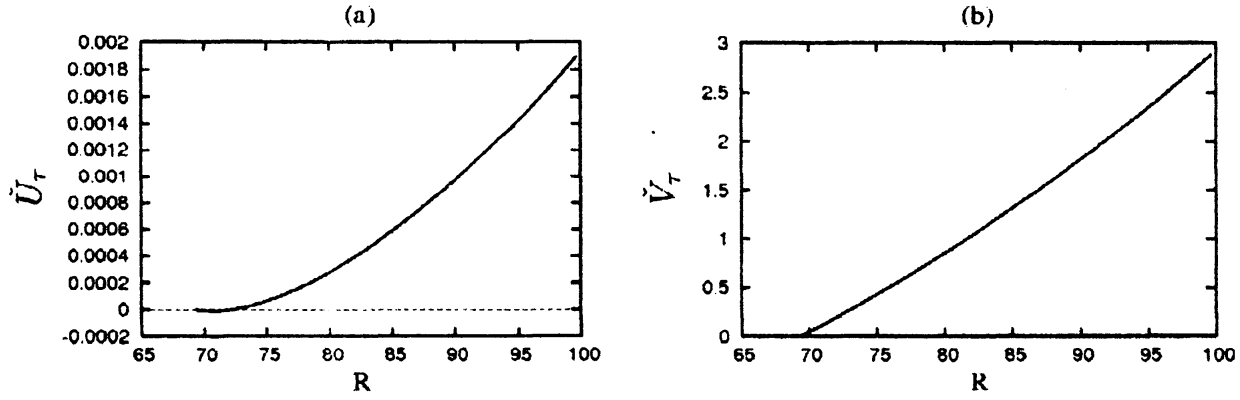

図 4: The momentum transports. (a): $\check{U}_\tau$ in the streamwise direction, (b): $\check{V}_\tau$ in the spanwise direction. α=0.35, β=2.36, Ω=140.

4.2 The nonlinear analysis

The bifurcation diagram for this system is depicted in Fig.3, where the phase speed c of the nonlinear solution is shown to bifurcate at $R = 69.39$ from the curve of $-\Re[\sigma]/\alpha$ for the linear disturbance.

Fig.4 represents the bifurcation nature of the nonlinear solution in terms of the momentum transports $\check{U}_\tau$ and $\check{V}_\tau$. It should be stressed that the momentum transport in the spanwise direction, which is absent in the basic laminar state, is generated in the three-dimensional travelling-wave solution travelling in the streamwise direction.

Although the mean flow modification $\check{U}(z)$ itself causes scarcely any changes in the total momentum transport $\frac{dU_B}{dz}|_{z=\pm 1} + \check{U}_\tau$ in the streamwise direction, the profile of the total mean flow $U_B + \check{U}$ is changed substantially as is shown in Fig.5(a) although the modification $\check{U}$ is still not sufficient to produce a inflection point. A part of the energy of the basic flow is transferred to three-dimensional disturbances and is spent partially to generate the mean flow $\check{V}$ in the spanwise direction. The generated mean flow $\check{V}$ in the spanwise direction (Fig.5(b)), the profile of which is anti-symmetric in z, amounts to a few percent of $U_B + \check{U}$ when their peak values are compared at the Reynolds number even about 50% above

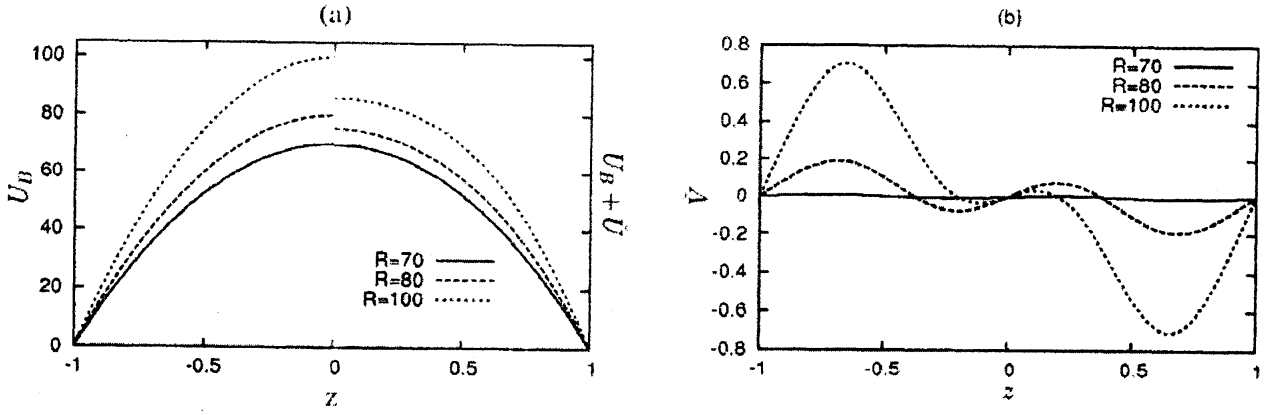

図 5: (a): The total mean flow $U_B + \check{U}$ in the streamwise direction. $-1 \leq z \leq 0$: undisturbed and $0 \leq z \leq 1$: disturbed. (b): The mean flow $\check{V}$ in the spanwise direction. $R = 70, 80, 100$ with α=0.35, β=2.36, Ω=140.

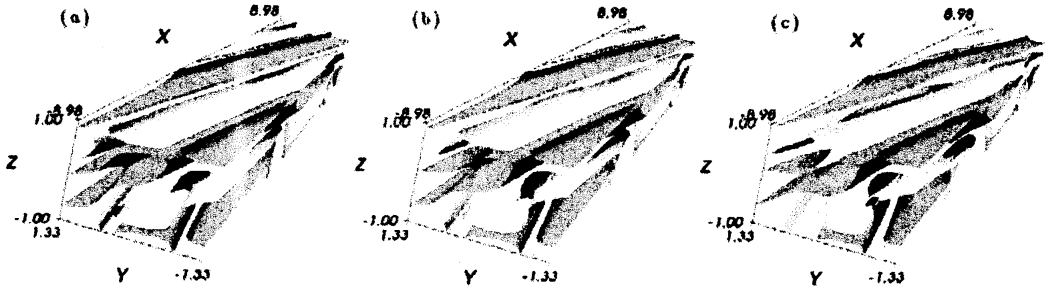

図 6: The equisurface $\omega = \omega_0$ of the streamwise component of the vorticity of the secondary flow with α=0.35, β=2.36, Ω=140. On the black surfaces $\omega = \omega_0$ and on the grey surfaces $\omega = -\omega_o$. (a): R=70, $\omega_0 = 1.70$ ($\omega_{max} = 6.81182$, $\omega_{min} = -6.81277$,), (b): R =80, $\omega_0 = 8.05$ ($\omega_{max} = 28.6589$, $\omega_{min} = -27.6400$), (c): $R = 100$, $\omega_0 = 16.05$ ($\omega_{max} = 49.6988$, $\omega_{min} = -45.9090$).

its critical value. The vorticity due to $\check{V}$ has the same sign as the background rotation Ω. The peaks of the spanwise mean flow profile in the direct numerical simulation by Oberlack *et al* (2006) are situated closer to the boundaries $z = \pm 1$ than our $\check{V}$ (see their figure 5). These differences are probably due to that fact that their Reynolds number $R_{e_\tau} = 180$ and the Coriolis parameter $R_o = 2.5, 6.0, 10.0$ are extremely large by our corresponding definitions: $R = \frac{1}{2}R_{e_\tau}^2 = 16,200$, $\Omega = R_{e_\tau}R_o = 450, 1,080, 1,800$. Nonetheless, it should be noted that the reverse flow nature of $\check{V}$ adjacent to the midplane $z = 0$ with three inflection points across the channel can also been seen in their direct numerical simulation results. The inflectional flow in the spanwise direction may lead to instabilities of the secondary flow and further bifurcations may ensue.

The flow field of the nonlinear travelling-wave solution throughout the channel is depicted in terms of the streamwise component of the vorticity, $\omega = \boldsymbol{i} \cdot \nabla \times \boldsymbol{u}$, in Fig.6. It can be seen that the vortex tubes are twisted more strongly as R is increased.

5 Conclusions

We have analysed the stability of plane Poiseuille flow subject to the streamwise system rotation. It is found that when rotation is added the instability due to two-dimensional perturbations is delayed. A further increase of rotation leads to three-dimensional instability whose critical Reynolds number is far less than the critical Reynolds number for non-rotating Poiseuille flow. We have also analysed the nonlinear aspect of the bifurcating three-dimensional secondary flow. The secondary flow exhibits a spiral vortex structure propagating in the streamwise direction with a spanwise anti-symmetric mean flow.

Investigation of the stability of the secondary flow is under way and detailed results will be reported separately in the near future. A preliminary analysis indicates that the secondary state can be stable for Reynolds numbers slightly above the critical value.

参考文献

[1] CHUNG, K. C. & ASTILL, K. N. 1977 Hydrodynamioc instability of viscous flow between rotating coaxial cylinders with fully developed axial flow. *J. Fluid Mech.* **81**, 641–655.

[2] COTREL, D. L. & PEARLSTEIN, A. J. 2004 The connection between centrifugal instability and Tollmien-Schlichting-like instability for spiral Poiseuille flow. *J. Fluid Mech.* **509**, 331–351.

[3] COTREL, D. L. & PEARLSTEIN, A. J. 2006 Linear stability of spiral and annular Poiseuille flow for small radius ratio. *J. Fluid Mech.* **547**, 1–20.

[4] IMSL, VISUAL NUMERIC INC. 1990 IMSL/Math Library. Digital Visual Fortran Professional Edition V6.0A, Digital Equipment Corporation Japan.

[5] HASOON, M. A. & MARTIN, B. W. 1977 The stability of viscous axial flow in an annulus with a rotating inner cylinder. *Proc. R. Soc. Lond.* **A352**, 351–380.

[6] JOSEPH, D. D. 1976 Stability of Fluid Motions, Vols I and II. Springer.

[7] MESEGUER, A. & MARQUES, F. 2002 On the competition between centrifugal and shear instabilitiy in spiral Poiseuille flow. *J. Fluid Mech.* **455**, 129–148.

[8] OBERLACK, M., CABOT, W., PETTERSSON REIF, B. A. & WELLER, T. 2006 Group analysis, direct numerical simulation and modelling of a turbulent channel flow with streamwise rotation. *J. Fluid Mech.* **562**, 383–403.

[9] RECKTENWALD, I., BRÜCKER, CH. & SCHRÖDER, W. 2004 PIV investigation of a turbulent channel flow rotating about the streamwise axis. *Advances in Turbulence X*, 561–564.

[10] TAKEUCHI, D. I. & JANKOWSKI, D. F. 1981 A numerical and experimental investigation of the stability of spiral Poiseuille flow. *J. Fluid Mech.* **102**, 101–126.

[11] WALL, D. P., & NAGATA, M. 2006 Nonlinear secondary flow through a rotating channel. *J. Fluid Mech.* **564**, 25–55.